

Article

The Line-of-Sight Analysis of Spatial Distribution of Galaxies in the COSMOS2015 Catalogue

Maxim Nikonov ¹, Mikhail Chekal ^{1,*}, Stanislav Shirokov ², Andrey Baryshev ³
and Vladimir Gorokhov ³

¹ The Moscow Institute of Physics and Technology, 1 “A” Kerchenskaya St., 117303 Moscow, Russia; maxnikonov007@gmail.com

² SPb Branch of Special Astrophysical Observatory of Russian Academy of Sciences, 65 Pulkovskoye Shosse, 196140 St. Petersburg, Russia; arhath.sis@yandex.ru

³ Department of Applied Mathematics, Saint Petersburg Electrotechnical University, Ulitsa Professora Popova 5, 197376 St. Petersburg, Russia; baryshev.andriy@gmail.com (A.B.); vlgorohov@mail.ru (V.G.)

* Correspondence: mishka.chekal@gmail.com

Received: 9 September 2020; Accepted: 18 November 2020; Published: 20 November 2020



Abstract: New observations of high-redshift objects are crucial for the improvement of the standard Λ CDM cosmological model and our understanding of the Universe. One of the main directions of modern observational cosmology is the analysis of the large-scale structure of Universe, in particular, in deep fields. We study the large-scale structure of the Universe along the line of sight using the latest version of the COSMOS2015 catalogue, which contains 518,404 high quality photometric redshifts of galaxies selected in the optical range of the COSMOS field ($2 \times 2 \text{ deg}^2$), with depth up to the redshift $z \sim 6$. We analyze large-scale fluctuations in the number of galaxies along the line of sight and provide an estimate of the average linear sizes of the self-correlating fluctuations (structures) in independent redshift bins of $\Delta z = 0.1$ along with the estimate of the standard deviation from homogeneity (the observed cosmic variance). We suggest a new method of the line-of-sight analysis based on previous works and formulate further prospects of method development. For the case of the theoretical form of approximation of homogeneity in the Λ CDM framework, the average standard deviation of detected structures from homogeneity is $\sigma_{\text{mean}}^{\Lambda\text{CDM}} = 0.09 \pm 0.02$, and the average characteristic size of structures is $R_{\text{mean}}^{\Lambda\text{CDM}} = 790 \pm 150 \text{ Mpc}$. For the case of the empirical approximation of homogeneity, the average standard deviation of detected structures from homogeneity is $\sigma_{\text{mean}}^{\text{empiric}} = 0.08 \pm 0.01$, and the average characteristic size of structures is $R_{\text{mean}}^{\text{empiric}} = 640 \pm 140 \text{ Mpc}$.

Keywords: cosmology; observations; large-scale structure of the universe

1. Introduction

The development of observational techniques and the increase of computing power at the beginning of the 21st century made it possible to study the evolution of large-scale structure of the Universe (LSSU) from the moment of birth of the first galaxies to the modern era. The relevance of theoretical models and the correct understanding of the evolution of the Universe is determined by using various observational cosmological tests [1–3].

The Λ CDM model is the standard cosmological model (SCM) that assumes the homogeneous distribution of matter in the Universe (“at sufficiently large scales”) including cold dark matter and dark energy. The SCM also implies the evolution of the density fluctuations of both dark and luminous matter with time, which is associated with the observed large-scale structure of the Universe. The SCM predicts that the primordial small density fluctuations of the dark and luminous matter

($\delta\rho/\rho \sim 10^{-5}$) have linear time-growth for the structures having scales larger ~ 10 Mpc at the present epoch [2,4]. The largest predicted by Λ CDM structures have sizes about the scale of the Baryon Acoustic Oscillations $R_{baO} \sim 100$ Mpc [5].

The very important observational test of the SCM is to estimate the maximum amplitudes and sizes of the largest structures visible in the high redshift Universe. This test can establish an observational limit to “the galaxy bias factor”, i.e., the ratio of fluctuation amplitudes of visible to dark matter [4]. Modern cosmological N-body simulations¹ provide MULTIDARK-GALAXIES catalogs, derived from the Planck cosmology MULTIDARK simulations MDPL2, with a volume of $1 h^{-1}\text{Gpc}^3$ and mass resolution of $1.5 \times 10^9 h^{-1}M_{\odot}$ by applying the semi-analytic models GALACTICUS, SAG, and SAGE [5]. These catalogs can be used for comparison between Λ CDM model predictions with real galaxy distribution at high redshift. In the next decade, the sensitivity limit of the upcoming telescopes (The James Webb Space Telescope², ALMA³, SKA⁴) will be sufficient to detect the earliest galaxies and hence to perform the “largest structure” observational test.

However, we can already estimate the amplitudes and sizes of visible matter fluctuations by using the deepest narrow-angle catalog COSMOS2015 [6], which contains more than 5×10^5 galaxies with high quality measured photometric redshifts up to $z = 6$.

The COSMOS2015 catalog is significantly improved compared with its previous version, used in the works by Nabokov and Baryshev [7,8], Shirokov et al. [9]. Note that in recent works, several structures were detected in the COSMOS field, which also point to existence of large filamentary structures at $z \sim 0.73$, called the COSMOS wall [10], structures at redshifts of $0.1 < z < 1.2$ [11], voids at $z \sim 2.3$ [12] and massive proto-supercluster at $z \sim 2.45$ [13]. The very large structure of the dark matter with a size of about 1000 Mpc was detected in the COSMOS field by using method of the weak gravitational lensing [14,15].

In this paper, we develop preceding approach used by Nabokov and Baryshev [7,8], Shirokov et al. [9]. We develop a new method of analysis of the galaxy number counts by introducing two-level of fluctuation sequences. We also use the last version of the COSMOS2015 catalogs.

2. The COSMOS2015 Catalogue

2.1. Description

In this paper, we use the COSMOS2015 catalogue [6] of precise photometric redshifts to analyze the line-of-sight distribution of galaxies. The catalog contains 30-band photometry data over the entire spectral range from radio to X-ray for 518,404 photometric redshifts of galaxies in the range $0 < z < 6$. The targets were selected in the optical range using the Hubble Space Telescope and were supplemented by data from the Chandra and XMM-Newton space observatories. The main goal of the COSMOS project is to study the relationships between the large-scale structure of Universe, dark matter, the formation of galaxies and the activity of nuclei in galaxies, as well as the influence of environmental conditions on the evolution of galaxies. The survey covers two square degrees on the celestial sphere nicknamed the COSMOS field in the direction of Sextans constellation.

2.2. Photometric Redshifts

Large catalogs of redshifts allow the usage of a wide range of statistical tools that provide estimates of systematic effects via cosmological tests (e.g., the LSSU, Hubble diagram, Malmquist bias, and gravitational lensing bias [16,17]). Conclusions about the LSSU drawn from careful analysis of

¹ <https://www.cosmosim.org>

² <https://www.jwst.nasa.gov>

³ <https://www.almaobservatory.org>

⁴ <https://www.skatelescope.org>

photometric redshifts are mostly in agreement with results obtained from spectral surveys and other independent studies (see, for example, Shirokov et al. [9], Sokolov et al. [18]).

However, relatively large errors in the photometric redshifts estimation make the study of the LSSU especially challenging. Essential improvements in photometric redshift techniques, using the best SED fitting in the COSMOS field imaged in a large number of filters [6] or deep learning methods [19], allow us to reach a redshift uncertainty $\sigma_z = 0.007(1+z)$ at small redshifts, which corresponds to a distance uncertainty of ~ 40 Mpc (at $z \sim 1$). At high redshifts $3 < z < 6$, the photometric redshifts in COSMOS2015 catalog are defined on the grid in steps of $\sigma_z < 0.021(1+z)$ [6] using *Hyperz: Photometric Redshift Code*⁵.

In our analysis, we take the linear size of the redshift bin $\Delta z = 0.1$, which is an order of magnitude larger than the redshift error $\sigma_z \sim 0.007$. So, we can firmly study the large-scale structures having linear sizes larger than ~ 100 Mpc.

2.3. Selection Effects

In the literature, there is no reliable theoretical estimate of all observational selection effects in construction of the number-distance relation. For example, the Malmquist bias is a result of the limited magnitude sensitivity of the equipment, which leads to preferable detection of the brighter sources. Such selection effects as K-corrections, evolution effects, types of continuous spectra of galaxies, must also be taken into account in directly observed quantities.

The usual approach for taking into account the main selection effects in the primary observed number-distance relation is to use a fitting function for the redshift distribution $N(z)$. We use several functional types of combined observational selection effects, including an exponential function for all redshifts, which decreases sharply with increasing redshift.

Photometric redshifts are determined by using simultaneously several filters, therefore, they are affected by the selection of visible magnitudes in different filters. This selection may contain the so-called “spectral deserts”, which are often found in spectroscopic observations. The description of this and other issues in detail, and the data processing decisions of the authors of the catalog is given in (Laigle et al. [6] [Section 3.2]). In the COSMOS2015 catalog, the observational selection effects (such as K-corrections, evolution effects, types of continuous spectra of galaxies and much more) have already been taken into account. Thus, we consider the catalog as a fair galaxy sample.

Figure 1 shows the angular distribution of 25,750 galaxies in the COSMOS2015 catalogue in a slice with thickness of $\Delta z = 0.2$ at $z = 1.0$. Each imaged galaxy has 1σ uncertainty $\sigma(z) < 10\%$. We can see the inhomogeneity of this distribution. The contrast between the medium pixels and the maximum pixels reaches a factor 3. The analysis of similar slices was performed in Chiang et al. [20]. Circular empty regions are a result of masking stars. Stars in the field greatly complicate the construction of 3D maps of galaxies, but does not affect the radial distribution along the line of sight on large scales (in redshift bins).

In the next section, we describe the method we used to analyze the LSSU by radial fluctuations of the number of galaxies along the line of sight.

⁵ https://www.researchgate.net/publication/258555988_Hyperz_Photometric_Redshift_Code

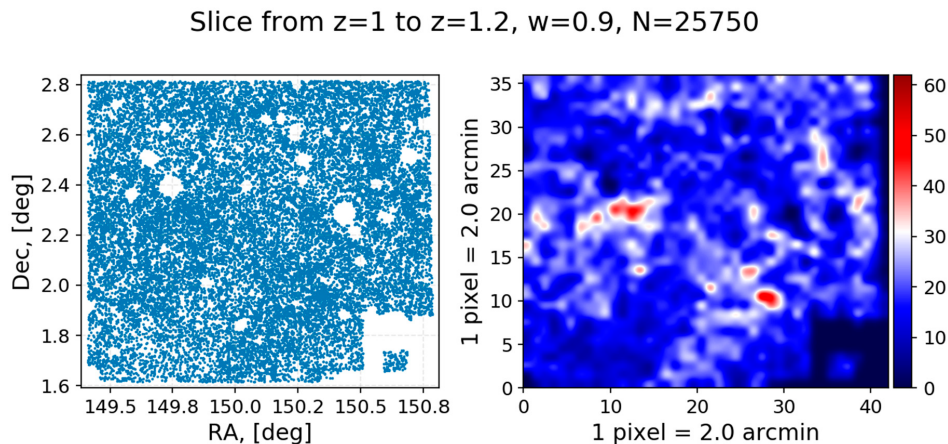


Figure 1. The projection on the sky of 25,750 galaxies from the COSMOS2015 catalogue in the range $1.0 < z < 1.2$ with the error $\sigma(z) < 10\%$. The left angular map shows galaxies as points. The right angular map is gaussian interpolation in 36×42 pixels (each of which is equal to 2 squared minutes) plotted by using the matplotlib.pyplot library. The color palette shows the galaxy count in one pixel.

3. The Method for Line-of-Sight Analysis of the LSSU in Spatial Bins

3.1. Spatial Distribution of Galaxies

According to the SCM, fluctuations in the large-scale distribution of galaxies could be approximated as a Gaussian process. Therefore, we assume that the histogram of the number of galaxies in spatial bins is described by a smooth function with a limited variance and an expected value (or average value) at each point. Moreover, this function starts to grow as $\sim R^D$, where R is the radius of probe sphere, and D is a certain density characteristic associated with the spatial correlation function of matter density. The quantity D can be also called the fractal dimension, assuming that the large-scale distribution of matter is naturally-hierarchical one created by the gravity influence [3]).

According to the N-body simulations in the evolutionary theory of galaxies formation frameworks, the average number of galaxies has a maximum at $z \sim 1$, but their mass and luminosity are less than at $z = 0$ [5]. In other words, the detection probability of a massive and bright (detectable) galaxy is a bit lower at $z \sim 1$ than at smaller redshifts. At large redshifts $z > 2$ the number of galaxies and their mass rapidly decrease. This result can be verified by the query interface on CosmoSim website⁶ by the MDPL2 catalogs [5]. Apparently, this is because small galaxies at $z \sim 1$ are being continuously merged by the influence of gravity and other evolution processes, forming more massive ones at $z = 0$. We also note that counts of simulated galaxies is a complicated issue and highly dependent on their detectability and detection methods. So, the work by Graziani et al. [21] shows how a smooth accretion can create MW-like galaxies at $z = 0$ in the overdense environment.

3.2. Radial Histogram of the Number of Galaxies

Deep surveys of galaxies are narrow-angle conical sections of the global spatial distribution of galaxies. The radial distribution of the number of galaxies $N_1(z)$ is given by the equation

$$dN(z, dz) = N_1(z)dz, \quad (1)$$

where dN is the number of galaxies in redshift range from z to $z + dz$ (linear density). We consider the dependence $N(z)$ as the histogram $\Delta N / \Delta z$. The number of galaxies $\Delta N(z, \Delta z)$ counted in a spherical shell with thickness of Δz such that

⁶ <https://www.cosmosim.org>

$$\Delta N(z, \Delta z) = N(z)\Delta z. \tag{2}$$

In other words, the $N(z)$ distribution is an observable approximation of the $N_1(z)$ distribution.

Thus, the distribution $N(z)$ can be built in redshift bins with a step of Δz . The value $\Delta N(z, \Delta z)$ is the number of galaxies in a spherical shell $(z, z + \Delta z)$. We conclude that with a reasonable choice of the parameter Δz , the observed histogram $\Delta N/\Delta z$ corresponds to the real radial distribution of the number of galaxies $N(z)$. In our case, the reasonable choice of the parameter Δz is bin $\Delta z = 0.1$.

3.3. The Approximations of Homogeneous Distribution

We approximate the homogeneous radial distribution of the number of galaxies with the least-squares method (LSM). Since the studied distribution has a high noise level (including the cosmic variance) and possible unknown systematic effects, the LSM via theoretical function may give an inaccurate result depending on the sample geometry. Therefore, the further introduced empirical functions as an alternative that can give a better approximation in the least-squares sense.

In the SCM frameworks, the distribution of galaxies $N(z)$ is approximated by a power law [22]

$$\Delta N_{\text{model}}(z, \Delta z) = A \left(\frac{z^a + z^{ab}}{z^b + C} \right) \Delta z, \tag{3}$$

where $N_{\text{model}}(z, \Delta z)$ is the number of galaxies in the redshift bin $(z, z + \Delta z)$. The formula has three free parameters for the LSM: a , b , and C .

We also used the empirical approximation function suggested in the works by Shirokov et al. [9], Massey et al. [15], Lovyagin [23]

$$\Delta N_{\text{emp1}}(z, \Delta z) = Az^\gamma e^{(-z/z_c)^\alpha} \Delta z, \tag{4}$$

where the free parameters γ , α , and z_c can be found by the LSM, and the dependent factor A is the normalization constant. The normalization constant is chosen such that the integral of function $N(z)$ is equal to the total number of galaxies N ,

$$\int_0^\infty N(z)dz = \int_0^\infty Az^\gamma \exp\left(-\left(\frac{z}{z_c}\right)^\alpha\right) dz = \frac{Az_c^{\gamma+1}\Gamma\left(\frac{\gamma+1}{\alpha}\right)}{\alpha} = N, \tag{5}$$

where $\Gamma(x)$ is the Euler’s complete gamma function. However, factor A cannot be calculated directly from the formula (5) due to the high noise level. Therefore, accordingly to Lovyagin [23], it is necessary to search for it in the range from $A - \sqrt{A}$ to $A + \sqrt{A}$.

In addition, we considered a particular case of the function (4) for $\alpha = 1$ and new labels for the parameters,

$$\Delta N_{\text{emp2}}(z, \Delta z) = Az^a e^{-bz} \Delta z, \tag{6}$$

to estimate the difference in the sum of LSM residuals between the three-parameter and two-parameter functions.

We searched for the coefficients using scipy library and leastsq function, which has two parameters: initial values of the parameters (input) and the sum of LSM residuals (output). A parametric vector $(10^4, 1, 1, 1)$, where the value 10^4 corresponds to parameter A in all approximation Formulas (3)–(6), was taken as a zero approximation for the parameters of all functions. We call the approximation ΔN_{model} as the theoretical one and the approximations ΔN_{emp1} and ΔN_{emp2} as the empirical ones. Since our analysis is based on the clear mathematical approach without an accurate physical interpretation of the approximation parameters, we will use quantities $\Delta N_{\text{approx1}}$, $\Delta N_{\text{approx2}}$, and $\Delta N_{\text{approx3}}$ instead of ΔN_{model} , ΔN_{emp1} , and ΔN_{emp2} .

3.4. The Fluctuation Amplitudes

After finding the best fitting parameters, we can detect inhomogeneities in the radial histogram of the observed number of galaxies. Fluctuations of physical quantities are the deviations of these quantities from their mean value, caused by random processes. The variance of fluctuations can be found in the plot of relative fluctuations, which we call the fluctuation pattern. We consider a fluctuation in each redshift bin $\delta(z, \Delta z)$ as follows

$$\delta(z, \Delta z) = (\Delta N_{\text{obs}} - \Delta N_{\text{approx}}) / \Delta N_{\text{approx}}, \tag{7}$$

where ΔN_{obs} is the observed number of galaxies in the bin, and ΔN_{approx} is the theoretically expected number of galaxies in the bin that is equal to the integral under the approximation function in the range $(z, z + \Delta z)$. The quantity ΔN_{approx} has the physical sense of the fluctuation mean and depends on the quality of the LSM approximation as well as the approximation formula.

One can introduce an index i denoting the ordinal number of the bin for the ΔN and δ values. Thus, δ_i is a relative difference between the observed number of galaxies and the theoretically expected one derived by the chosen approximation function of homogeneous distribution of galaxies in the i -bin.

We take the sequence of fluctuations δ_i only with either positive or negative values as a criterion for detecting structure in the fluctuation pattern. So, we can introduce a new index j as the ordinal number of the detected structure. We denote the middle of the first bin of each such sequence as z_{start} and the middle of the last bin as z_{final} . Each j -structure has the final bin, which is the start bin for $j + 1$ -structure except for the last one. We denote all such transition bins as j -bins. The last structure with the index $j = m + 1$ has $z_{\text{final}} \approx z_{\text{max}}$, where z_{max} is the size of galaxy sample. We exclude this structure from analysis. Thus, we detect m structures that we now consider as a new random process of candidates for large-scale structures of galaxies.

We introduce quantity δ_j as the average value over all fluctuations δ_i of j -structure by the equation

$$\delta_j = \sum_{i \in j} \delta_i / n, \tag{8}$$

where n is the number of i -bins inside j -structure. In this paper, we consider structures with $n > 2$. This leads to the fact that the redshift size of detectable structures is greater than $\Delta z = 0.2$ in redshift radial space. Further, we calculate an unbiased estimate of the variance of observed fluctuations of the number of galaxies s_j^2 and a variance of the sample mean $\hat{\sigma}_{\delta_j}^2$ for each structure by the equations ([24], p. 670, Equations (2)–(8) and (19)).

$$s_j^2 = \sum_{i \in j} (\delta_i - \delta_j)^2 / (n - 1), \tag{9}$$

$$\hat{\sigma}_{\delta_j}^2 = \frac{s_j^2}{n}, \tag{10}$$

where n is the number of i -bins inside j -structure. From now on, we will use designations σ instead of $\hat{\sigma}$ as estimate of variance and σ_{obs} instead of $|\delta_j|$ as the mean value of observed fluctuations of j -structure.

The mean value of observed fluctuations over all structures σ_{mean} can be found as follows

$$\sigma_{\text{mean}} = \overline{\sigma_{\text{obs}}} = \sum_{j=1}^m \frac{|\delta_j|}{m} = \sum_{j=1}^m \frac{\sigma_{\text{obs}}}{m}, \tag{11}$$

where m is the number of detected j -structures.

We can obtain an error of the mean value of observed fluctuations over all structures $\sigma_{\sigma_{\text{mean}}}$, taking into account the Poisson noise, by the formula

$$\sigma_{\sigma_{\text{mean}}}^2 = \sigma_{\sigma_{\text{obs}}}^2 + \frac{(\overline{\sigma_{\text{P}}})^2}{m}, \tag{12}$$

where $\sigma_{\sigma_{\text{obs}}}$ is the standard deviation of σ_{mean} , obtained similarly to $\sigma_{\sigma_{\text{obs}}}$ by Equations (9) and (10), $\overline{\sigma_{\text{P}}}$ is the average Poisson noise over all structures, and m is the number of detected j -structures. Such approach to Poisson errors impairs the estimate of the mean error of the observed cosmic variance, but allows one to detect possible structures in a sample with a signal-to-noise ratio less than unity (see, for example, Figures 6 and 7 from Shirokov et al. [9]). We can do this because the amplitude of the Poisson errors varies weakly within a single sample of galaxies with a factor of about 2–3.

We rename σ_{obs} as an amplitude of fluctuations of the observed number of galaxies or just the fluctuation amplitude in the context of one structure and σ_{mean} as an average fluctuation amplitude over all detected structures in the context of the galaxy sample.

3.5. Comparison with the SCM Predictions

According to the Λ CDM model, the theoretical cosmic variance of the fluctuations in the density of matter σ^2 for each redshift bin $(z, z + \Delta z)$ is equal to the sum of two variances,

$$\sigma^2(z, \Delta z) = \sigma_{\text{gal}}^2 + \sigma_{\text{p}}^2, \tag{13}$$

where σ_{p}^2 is the classical Poisson noise, and σ_{gal}^2 is the variance calculated by the formula

$$\sigma_{\text{gal}}^2(V) = \frac{1}{(1+z)V^2} \int_V dV_1 \int_V dV_2 \zeta_{\text{gal}}(|\mathbf{r}_1 - \mathbf{r}_2|), \tag{14}$$

where $V = V(z, \Delta z)$ is the integration volume, $\zeta(|\mathbf{r}_1 - \mathbf{r}_2|)$ is the spatial two-point correlation function of matter density, and the factor $1/(1+z)$ takes into account the linear growth over time of the fluctuations of LSSU [7]. In fact, this formula corresponds to the complete correlation function of matter (visible and dark). However, within the SCM frameworks, the one is derived only for dark matter, which is associated with the visible matter via the hypothesis of galaxy bias [4]. Various parameters of galaxies should be taken into account in order to better match the theory of dark matter with observations of baryonic matter [4].

The variance of density fluctuations of dark matter is given by Equations (10) and (12) from Moster et al. [4] or by the formula

$$\sigma_{\text{dm}}(z, \Delta z) = \frac{\sigma_a}{z^\beta + \sigma_b} \sqrt{\frac{0.2}{\Delta z}}, \tag{15}$$

where parameters $(a, b, \text{ and } \beta)$ are related to the angular dimensions of the COSMOS field and are equal to (0.069, 0.234, and 0.834), respectively [4].

The galaxy bias has theoretical and observed values, which may differ from each other. For example, the accounting for the stellar mass of visible galaxies reduces the bias difference (as difference between theoretical and observed values) with the factor of 2–3 [9]. Both values are defined as a ratio of the correlation function of visible matter to the one of dark matter. The ratio of “visible variance” to “dark variance” can be used as a calculable approximation of galaxy bias, $b^2(z, m_\star, \dots) = \zeta_{\text{gal}}/\zeta_{\text{dm}} \approx \sigma_{\text{gal}}^2/\sigma_{\text{dm}}^2$, which can be estimated from observations (with adding the “obs” prefix) and corrected for Poisson noise [9]. Galaxy bias is a complicated function that depends on a large number of parameters and redshift effects. If the observed function of galaxy bias is coincided with the theoretical one, $b_{\text{obs}}(z)/b(z, m_\star, \dots) \approx 1$, then the bias hypothesis is confirmed.

In this work, we calculate only the observed bias value $b_{\text{obs}}(z)$. The average bias b_{mean} (as the output method's parameter) demonstrates the effect of difference between the observed variance of visible matter and theoretical variance of dark matter in the galaxy sample. We calculate the average bias value over structures as follows

$$b_{\text{mean}} = \bar{b} = \frac{\sum b_j}{m}, \tag{16}$$

where m is the number of structures detected in the fluctuation pattern. We take an error for b_j as the relative error of the value σ_{obs} and its error, respectively. The estimate of error $\sigma_{b_{\text{mean}}}$ is the standard deviation of b_{mean} .

According to the Formula (13), it is necessary to take into account the Poisson noise ($\sigma_{\text{P}}^2 = 1/\Delta N$) when we calculate the observed bias value. The noise may be too high on poor samples (with $\Delta N < 10^4$). A poor sample may give a small fluctuation amplitude $\delta_{\text{obs}}(z, \Delta z)$ relatively to a large Poisson background σ_{P} that will lead to a negative observed variance σ_{obs} . In this paper, we eliminate such structures.

3.6. Alternative Approach

The observed distribution of galaxies is consistent with the power-law nature of the correlation function of matter density $\xi_{\text{pl}}(r) = (r_0/r)^\gamma$ (e.g., Shirokov et al. [9], Tekhanovich and Baryshev [25]). Using Equation (14), one can calculate a power-law estimate of the cosmic variance ($\sigma_{\text{gal}} = \sigma_{\text{pl}}$) with the parameters $\gamma = 1, r_0 = 5$ from Shirokov et al. [9] as follows

$$\sigma_{\text{pl}}^2(V, r_0, \gamma) = \frac{1}{(1+z)V^2} \int_V dV_1 \int_V dV_2 \xi(|\mathbf{r}_1 - \mathbf{r}_2|, r_0, \gamma), \tag{17}$$

and compare its with the observed variance corrected for Poisson noise by introducing the power-law bias function $b_{\text{pl}}(z) = \sigma_{\text{obs}}/\sigma_{\text{pl}}$. The consistency between the power-law and observed bias functions, $b_{\text{obs}}(z)/b_{\text{pl}}(z) \approx 1$, will show the efficiency of applying the power-law correlation function (PLCF) without taking into account the influence of different selection effects for estimating the observed cosmic variance. This conclusion may be important for future testing of new cosmological models. We also get the average value of the power-law bias function \bar{b}_{pl} as the output method's parameter and its standard deviation $\sigma_{\bar{b}_{\text{pl}}}$.

3.7. Calculating the Fluctuation Scales

The metric distance in terms of redshift in the SCM is given by the formula

$$r(z)_{\text{Mpc}} = \frac{c}{H_0} \int_0^z \left(\Omega_v + \Omega_m^3(1+z) \right)^{-\frac{1}{2}} dz, \tag{18}$$

where c is the speed of light, $H_0 = 70 \text{ km s}^{-1} \text{ Mpc}^{-1}$ is the Hubble constant, the vacuum density (dark energy) $\Omega_v = 0.7$, the matter density (visible and dark) $\Omega_m = 1 - \Omega_v = 0.3$, and z is the source redshift. Since we are working in the co-moving space we will use the metric distance, not the luminosity distance.

Here, we introduce a more stringent criterion to estimate the linear scales of large-scale structures than it was used in the papers by Nabokov and Baryshev [7], Shirokov et al. [9]. As it is noted above, we calculate the structure borders z_{start} and z_{finish} as the middle of j -bins, where the fluctuation function δ_i changes a sign. The structure size R_j is given by the equation

$$R_j = \Delta r(z, \Delta z) = r(z_j^{\text{finish}}) - r(z_{j-1}^{\text{start}}), j \in (1, 2, \dots), \tag{19}$$

where the values z_j and z_{j+1} correspond to the midpoints of the j -bins ($z_0^{\text{start}} = 0$). We define the upper and lower errors of the structure size as half of the corresponding metric sizes of the start and final j -bins.

Since we are interested in average values of the target variables for a galaxy sample, we also calculate the average size of the detected structures $R_{\text{mean}} = \overline{R}_j$. The errors of R_{mean} take into account both the root-mean-square deviation from the mean, and the half sizes of the boundary bins by the formula

$$\sigma_{R_{\text{mean}}}^2 = \sigma_{\overline{R}_j}^2 + (\overline{\sigma_{R_j}})^2, \tag{20}$$

where $\sigma_{\overline{R}_j}$ is the standard deviation of R_{mean} , and $\overline{\sigma_{R_j}}$ is the mean of upper (or, respectively, lower) R_j errors.

According to the SCM, the correlation function of spatial density of dark matter is equal to zero at the scale of $r_0 = 174$ Mpc, $\xi_{\text{gal}}(174 \text{ Mpc}) = 0$, without reference to the galaxy bias value [26]. The bins with sizes exceeding this value can be considered as independent and requiring a sign change of the observed fluctuations $\delta_i = \delta_{\text{obs}}(z, \Delta z)$ on a scale about the double one $2r_0 \sim 350$ Mpc. Modern cosmological N-body simulations, such as the Horizon Run 2 simulation, predict inhomogeneities with a size of about 300 Mpc for the brightest galaxies, which are modelled over dark matter halos [27]. The BLUETIDES simulation, in which galaxies are modeled by simulating gas, shows the clustering galaxies at high redshifts with the galaxy bias $b \approx 8$ [28].

A comparison of metric distances $r(z)$ (comoving space) and luminosity distances $d_L = (1+z)r(z)$ (proper space) is shown in Table 1 for redshift bins $\Delta z = 0.1$, which are denoted by the midpoints \bar{z} . The difference between the corresponding distances caused by the factor $(1+z)$.

Table 1. The metric size of bins $\Delta z = 0.1$ in Mpc at various redshifts. $\Delta r(z)$ is the size in the moment $t = t(z)$ (comoving distances), and Δd_L is the size in the moment $t = t(0)$ (proper distances).

\bar{z}	0.05	0.95	1.45	1.55	1.65	1.95	2.95	3.95	4.95	5.95
$\Delta r(z, \Delta z)$, Mpc	407	244	184	175	166	144	95	68	52	41
$\Delta d_L(z, \Delta z)$, Mpc	448	784	866	879	890	920	989	1032	1063	1087

3.8. Applications of the Method

The methods of LSSU analysis should be maximally reliable and robust for any geometries. This way, for example, the sample depth should not significantly affect the identified structures, as we show in Appendix A for two disjoint samples of the COSMOS and UltraVISTA galaxies from the COSMOS2015 catalog. Besides, though we did not require a correlation between two disjoint samples, one can see a correlation for several structures at small redshifts that indicates their presence.

It is possible to consider density fluctuations of matter in metric space (with and without taking into account the temporal effects) instead of redshift space. In such a configuration, the uniform radial density distribution grows as a power-law function of the radius and, after reaching a maximum, also falls as one (with a negative exponent). However, for the transition from redshifts to metric distances, it is necessary to accept a certain cosmological model. We get different distances and cosmic variance in different cosmological models. It means that we need to calculate the fluctuation tables in a grid of models with a search for the optimum cosmological parameters. An illustration of a metric radial histogram in the Λ CDM model frameworks with a uniform approximation for the UltraVISTA subsample is given in Appendix B.

4. Results

4.1. Entire Sample of the COSMOS2015 Catalogue

Figure 2 (left) shows the radial histogram of the number of galaxies in the COSMOS2015 catalogue (without additional sampling) at all redshifts $0 < z < 6$ for 518,404 galaxies. The LSM approximations

are shown by dashed lines: red corresponds to the theoretical Formula (3), green to the empirical Formula (4), orange to its simplified form of Equation (6). The legend presents approximation formulas with coefficient values, and the root of the residual sum. The fluctuation pattern is shown in the right panel of Figure 2. Our LSM analysis gave a coincidence of the green and orange curves with high accuracy so that they can be considered as equivalent ones.

On the one hand, as it can be seen in the figure, the curves of the empirical cases coincide. This implies that the Formula (6) is successfully simplified. However, the presence of two parameters in the exponent leads to the uncertainty of determining the coefficients, which can result in the nonphysical large values of parameters. On the other hand, a power-law theoretical curve corresponding to Formula (3) has a similar behavior at small redshifts, but describes the histogram at high redshifts poorly.

At small redshifts, $z < 1.5$, both approximations give a mutually consistent result with an average fluctuation amplitude of $\delta \approx 10\%$ and an average structure scale of $\Delta R \approx 700$ Mpc. At intermediate redshifts, $1.5 < z < 3.5$, a difference between the empirical and theoretical approximations is increasing. At large redshifts, $3.5 < z < 6$, the difference grows rapidly, as well as a difference between the histogram and the approximations themselves that indicates an unsuccessful approximation of the histogram at these scales. This effect can be related to a lack of statistics at the highest redshifts or with unknown redshift systematics.

Nevertheless, in the fluctuation pattern, the regions of deficiency and excess of galaxies with a scale of 3–5 redshift bins are clearly visible. It can be noted that the fluctuations δ_i of the empirical curves are more stable with respect to redshift around $\delta \sim 10\%$ in the range $0 < z < 5$. That emphasises the importance of choosing the distribution maximum and a successful approximation of the distribution tail.

The fluctuation pattern, obtained from the analysis of the entire COSMOS2015 catalog, is similar to periodic density oscillations, which can be also seen in the deep-UltraVISTA sample in Appendix B (in metric space).

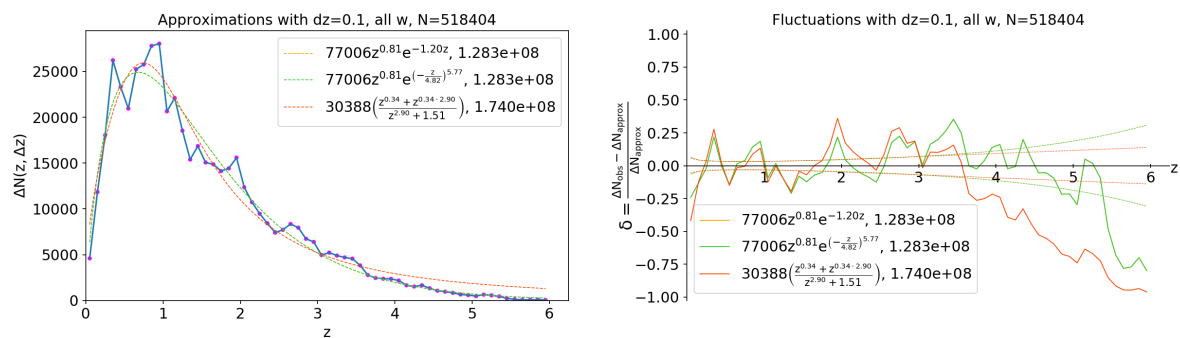


Figure 2. (left) Histogram of the radial distribution of photometric redshifts from the COSMOS2015 catalogue in the range $0 < z < 6$ for 518,404 galaxies within bins $\Delta z = 0.1$, and the approximations. Dotted lines mark the least-squares fittings. (right) The fluctuation pattern. Dotted lines mark Poisson noise 5σ .

4.2. The w -Sampling

To account for the photometric redshift uncertainties, we introduce the sampling parameter w , which is equal to the difference of one and the relative error in determining z ,

$$w_i = 1 - \frac{\sigma_i(z)}{z_i}, \quad i = 1, 2, \dots, N, \quad (21)$$

where $\sigma_i(z)$ is 1σ uncertainty of each redshift z_i and $N = 518,404$. Based on the choice of the parameter w , we considered four samples from the COSMOS2015 catalogue:

- any w (no sampling), i.e., the entire sample;
- $w > 0.7$ (weak sampling), i.e., galaxies with relative error $\sigma(z) < 30\%$ at significance level of 1σ or $\sigma(z) < 90\%$ at significance level of 3σ ;
- with $w > 0.9$ (medium sampling), i.e., galaxies with relative error $\sigma(z) < 10\%$ at significance level of 1σ or $\sigma(z) < 30\%$ at significance level of 3σ ;
- with $w > 0.97$ (strong sampling), i.e., galaxies with relative error $\sigma(z) < 3\%$ at significance level of 1σ or $\sigma(z) < 9\%$ at significance level of 3σ .

The high-resolution histograms of the radial distribution of the COSMOS2015 galaxies for the selection parameter w are shown in Figure 3. The left panel demonstrates how the selection by the quality of photometric redshifts reduces the number of galaxies and reveals the large-scale structures, for example, at $2 < z < 4$ in redshift space. The right panel is the left plot but in metric space, where distance units are in Mpc. We can see various structures (on Gpc scales) as a sum of the physics of the LSSU and observational selection effects.

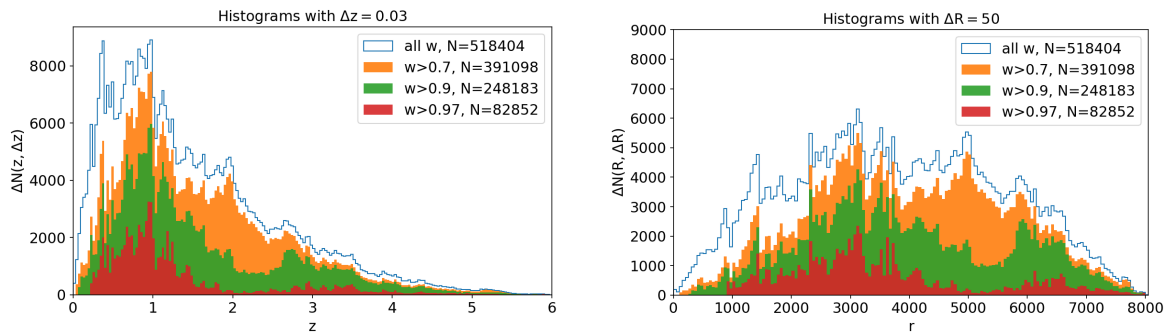


Figure 3. High resolution differential histograms of radial distribution of galaxies from the COSMOS2015 catalogue in redshift space (**left**) with $\Delta z = 0.03$, and metric space (**right**) with $\Delta r(z) = 50$ Mpc for the various values of the sampling parameter w .

Figure 4 (left panels) shows the histograms of the radial distribution of galaxies for sampling parameters $w = 0.7$ and $w = 0.9$ and demonstrates that reducing the sample based on the quality of photometric redshift helps to reveal the LSSU, for example, at $2 < z < 4$ with scale of about Gpc. In this way, the method can be also applied not only in the redshift space, but also in the metric space (see Appendix B).

For weak sampling ($w = 0.7$), the fluctuation pattern differs slightly from the entire sample, and the number of galaxies is about 75% of the total number. The empirical approximation describes the observed histogram better up to $z \approx 5$, while the theoretical curve is successful only up to $z \approx 3$.

For strong sampling ($w = 0.9$), the large-scale structures are seen more clearly, and the number of galaxies is about 48% of the total number. The empirical approximation describes the observed histogram poorly, while the theoretical curve has the smallest sum of residual squares. In this case, the region of galaxy deficiency (void) in the redshift range $2 < z < 2.5$, and the region of galaxy excess (supercluster) in the range $2.5 < z < 3.5$ are clearly visible.

It is important to note that for samples with more strictly selected photometric redshifts, the empirical Formula (6) predicts an underdensity at large redshifts, while the theoretical Formula (3) gives the best result.

We present the structure parameters detected by the method from the corresponding fluctuation patterns for the four values of w ($w = \text{“all”}$ means the case of no sampling) in Table 2 for empirical approximations of homogeneity (that are coincided), and in Table 3 for the theoretical curve. The description of structure table contents in detail is given in Section 3 and Appendix A.

The structure tables indicate the existence of physical large-scale structures in Gpc scales. The largest structures found in the COSMOS2015 catalogue are detected at redshifts: $2 \lesssim z \lesssim 2.5$ (void), and $2.5 \lesssim z \lesssim 3.5$ (cluster).

The main output of the tables is the characteristic size of structures R_{mean} and their average characteristic amplitude σ_{mean} . We obtain the galaxy bias functions $b(z)$ and the average bias b_{mean} through comparison of the predicted cosmic variances in different models with the observations. These parameters are convenient for fast comparison of different samples of galaxies.

The structure tables show that the observed cosmic variance can be described by the PLCF of density $\zeta(r) = (r_0/r)^\gamma$ with parameters $\gamma = 1.0$, $r_0 = 5$ at all redshifts [7,9,25]. The PLCF bias b_{pl} is greater than the dark matter bias b_{dm} in factor about 2–3.

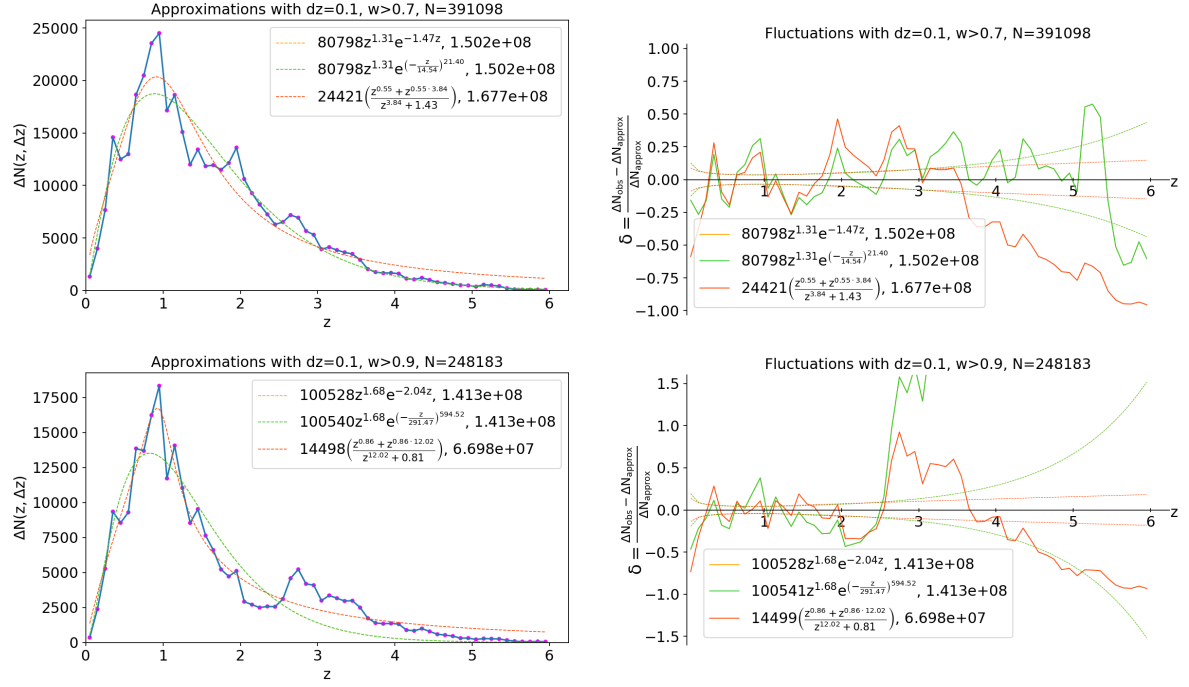


Figure 4. Histograms of radial distribution of the photometric redshifts and corresponding fluctuation patterns for samples with the parameter $w = 0.7$ for 391,098 galaxies (**top**), and $w = 0.9$ for 248,183 galaxies (**bottom**) with a bin $\Delta z = 0.1$. The dashed lines indicate the least squares fit (**left**) and Poisson noise 5σ (**right**).

Table 2. Tables of structures for w -samples from the COSMOS2015 catalogue for a bin $\Delta z = 0.1$ with $z_{\text{max}} = 6$ and the various σ_z selection. The approximation is by empirical Formula (6). In the last string there are the means of corresponding values (by all structures): mean of redshifts \bar{z}_{mean} , mean of structure sizes in Mpc R_{mean} , mean of Poisson noise level $\overline{1\sigma_{\text{p}}}$, mean of observed cosmic variance σ_{mean} , mean of dark matter variance $\overline{\sigma_{\text{dm}}}$, mean of dark matter bias $\overline{b_{\text{dm}}}$, mean of Peebles correlation function variance $\overline{\sigma_{\text{pl}}}$ and its bias $\overline{b_{\text{pl}}}$ (see details in the text).

Sample	j	n	\bar{z}	$\Delta r(z)$, Mpc	σ_{p}	σ_{obs}	σ_{dm}	b_{dm}	σ_{pl}	b_{pl}
COSMOS2015	1	3	0.15 ± 0.10	774^{+203}_{-183}	0.005	0.131 ± 0.064	0.188	0.7 ± 0.3	0.199	0.7 ± 0.3
$z_{\text{max}} = 6$	2	3	0.35 ± 0.10	694^{+183}_{-163}	0.004	0.065 ± 0.077	0.132	0.5 ± 0.6	0.179	0.4 ± 0.4
$w = \text{all}$	3	3	0.55 ± 0.10	618^{+163}_{-145}	0.004	0.044 ± 0.050	0.104	0.4 ± 0.5	0.168	0.3 ± 0.3
	4	5	0.85 ± 0.20	1035^{+145}_{-114}	0.003	0.058 ± 0.049	0.097	0.6 ± 0.5	0.188	0.3 ± 0.3
	5	8	1.50 ± 0.35	1265^{+108}_{-75}	0.003	0.072 ± 0.028	0.073	1.0 ± 0.4	0.187	0.4 ± 0.2
	6	4	2.00 ± 0.15	421^{+75}_{-65}	0.004	0.072 ± 0.050	0.050	1.4 ± 1.0	0.151	0.5 ± 0.3
	7	5	2.35 ± 0.20	482^{+65}_{-55}	0.005	0.058 ± 0.022	0.048	1.2 ± 0.5	0.156	0.4 ± 0.1
	8	12	3.10 ± 0.55	1000^{+55}_{-37}	0.004	0.162 ± 0.033	0.045	3.6 ± 0.7	0.168	1.0 ± 0.2
	9	5	3.95 ± 0.20	273^{+36}_{-32}	0.010	0.059 ± 0.039	0.032	1.8 ± 1.2	0.140	0.4 ± 0.3
	10	4	4.40 ± 0.15	180^{+31}_{-28}	0.014	0.050 ± 0.055	0.028	1.7 ± 1.9	0.129	0.4 ± 0.4
	11	7	4.85 ± 0.30	321^{+28}_{-24}	0.013	0.126 ± 0.046	0.030	4.2 ± 1.5	0.145	0.9 ± 0.3
means:			2.19 ± 0.22	642^{+148}_{-137}	0.006	0.082 ± 0.012	0.075	1.6 ± 0.4	0.164	0.5 ± 0.1

Table 2. Cont.

Sample	j	n	\bar{z}	$\Delta r(z)$, Mpc	σ_p	σ_{obs}	σ_{dm}	b_{dm}	σ_{pl}	b_{pl}
COSMOS2015 $z_{max} = 6$ $w = 0.7$	1	3	0.15 ± 0.10	774^{+203}_{-183}	0.008	0.195 ± 0.035	0.188	1.0 ± 0.2	0.199	1.0 ± 0.2
	2	3	0.35 ± 0.10	694^{+183}_{-163}	0.005	0.039 ± 0.116	0.132	0.3 ± 0.9	0.179	0.2 ± 0.6
	3	3	0.55 ± 0.10	618^{+163}_{-145}	0.005	0.101 ± 0.080	0.104	1.0 ± 0.8	0.168	0.6 ± 0.5
	4	5	0.85 ± 0.20	1035^{+145}_{-114}	0.003	0.135 ± 0.069	0.097	1.4 ± 0.7	0.188	0.7 ± 0.4
	5	8	1.50 ± 0.35	1265^{+108}_{-75}	0.003	0.110 ± 0.036	0.073	1.5 ± 0.5	0.186	0.6 ± 0.2
	6	4	2.00 ± 0.15	421^{+75}_{-65}	0.005	0.078 ± 0.055	0.050	1.5 ± 1.1	0.151	0.5 ± 0.4
	7	5	2.35 ± 0.20	482^{+65}_{-55}	0.005	0.042 ± 0.022	0.048	0.9 ± 0.5	0.156	0.3 ± 0.1
	8	12	3.10 ± 0.55	1000^{+35}_{-37}	0.005	0.189 ± 0.035	0.045	4.2 ± 0.8	0.168	1.1 ± 0.2
	9	3	3.75 ± 0.10	145^{+37}_{-35}	0.013	0.010 ± 0.017	0.028	0.0 ± 0.0	0.118	0.0 ± 0.0
	10	4	4.00 ± 0.15	202^{+35}_{-32}	0.013	0.092 ± 0.059	0.030	3.0 ± 1.9	0.131	0.7 ± 0.4
	11	7	4.55 ± 0.30	347^{+31}_{-26}	0.014	0.116 ± 0.044	0.031	3.7 ± 1.4	0.147	0.8 ± 0.3
	12	5	5.25 ± 0.20	193^{+25}_{-23}	0.025	0.269 ± 0.164	0.026	10.3 ± 6.3	0.134	2.0 ± 1.2
means:			2.37 ± 0.21	598^{+144}_{-134}	0.009	0.115 ± 0.022	0.071	2.6 ± 0.8	0.160	0.8 ± 0.2
COSMOS2015 $z_{max} = 6$ $w = 0.9$	1	3	0.15 ± 0.10	774^{+203}_{-183}	0.010	0.260 ± 0.108	0.188	1.4 ± 0.6	0.199	1.3 ± 0.5
	2	4	0.50 ± 0.15	955^{+173}_{-145}	0.005	0.054 ± 0.086	0.124	0.4 ± 0.7	0.192	0.3 ± 0.5
	3	5	0.85 ± 0.20	1035^{+145}_{-114}	0.004	0.118 ± 0.080	0.097	1.2 ± 0.8	0.188	0.6 ± 0.4
	4	3	1.15 ± 0.10	434^{+114}_{-102}	0.005	0.011 ± 0.073	0.066	0.2 ± 1.0	0.149	0.1 ± 0.4
	5	14	1.90 ± 0.65	1958^{+102}_{-55}	0.003	0.196 ± 0.043	0.066	3.0 ± 0.7	0.189	1.0 ± 0.2
means:			0.91 ± 0.24	1031^{+302}_{-287}	0.005	0.128 ± 0.046	0.108	1.2 ± 0.5	0.183	0.7 ± 0.2
COSMOS2015 $z_{max} = 6$ $w = 0.97$	1	3	0.35 ± 0.10	694^{+183}_{-163}	0.011	0.290 ± 0.173	0.132	2.2 ± 1.3	0.179	1.6 ± 1.0
	2	5	0.65 ± 0.20	1166^{+163}_{-129}	0.006	0.089 ± 0.055	0.114	0.8 ± 0.5	0.196	0.5 ± 0.3
	3	3	0.95 ± 0.10	487^{+129}_{-114}	0.007	0.120 ± 0.229	0.075	1.6 ± 3.1	0.153	0.8 ± 1.5
	4	3	1.35 ± 0.10	388^{+102}_{-92}	0.010	0.041 ± 0.135	0.059	0.7 ± 2.2	0.144	0.3 ± 0.9
	5	9	1.85 ± 0.40	1216^{+92}_{-62}	0.010	0.231 ± 0.074	0.064	3.6 ± 1.2	0.182	1.3 ± 0.4
means:			1.03 ± 0.18	790^{+227}_{-212}	0.009	0.154 ± 0.046	0.089	1.8 ± 0.5	0.171	0.9 ± 0.3

Table 3. Tables of structures for w -samples from the COSMOS2015 catalogue for a bin $\Delta z = 0.1$ with $z_{max} = 6$ and the various σ_z selection. The approximation is by theoretical formula (3). In the last string there are the means of corresponding values (by all structures): mean of redshifts \bar{z}_{mean} , mean of structure sizes in Mpc \bar{R}_{mean} , mean of Poisson noise level $1\bar{\sigma}_p$, mean of observed cosmic variance $\bar{\sigma}_{mean}$, mean of dark matter variance $\bar{\sigma}_{dm}$, mean of dark matter bias \bar{b}_{dm} , mean of Peebles correlation function variance $\bar{\sigma}_{pl}$ and its bias \bar{b}_{pl} (see details in the text).

Sample	j	n	\bar{z}	$\Delta r(z)$, Mpc	σ_p	σ_{obs}	σ_{dm}	b_{dm}	σ_{pl}	b_{pl}
COSMOS2015 $z_{max} = 6$ $w = all$	1	3	0.15 ± 0.10	774^{+203}_{-183}	0.005	0.169 ± 0.133	0.188	0.9 ± 0.7	0.199	0.9 ± 0.7
	2	3	0.35 ± 0.10	694^{+183}_{-163}	0.004	0.110 ± 0.084	0.132	0.8 ± 0.6	0.179	0.6 ± 0.5
	3	4	0.60 ± 0.15	900^{+163}_{-137}	0.003	0.038 ± 0.038	0.112	0.3 ± 0.3	0.186	0.2 ± 0.2
	4	4	0.90 ± 0.15	753^{+137}_{-114}	0.003	0.023 ± 0.057	0.087	0.3 ± 0.6	0.174	0.1 ± 0.3
	5	7	1.35 ± 0.30	1172^{+114}_{-83}	0.003	0.076 ± 0.027	0.077	1.0 ± 0.4	0.186	0.4 ± 0.1
	6	8	2.00 ± 0.35	989^{+83}_{-60}	0.003	0.114 ± 0.041	0.059	1.9 ± 0.7	0.176	0.6 ± 0.2
	7	7	2.75 ± 0.30	616^{+57}_{-45}	0.005	0.134 ± 0.048	0.046	2.9 ± 1.1	0.161	0.8 ± 0.3
	8	6	3.30 ± 0.25	420^{+45}_{-38}	0.006	0.082 ± 0.026	0.039	2.1 ± 0.7	0.151	0.5 ± 0.2
means:			1.42 ± 0.21	790^{+155}_{-137}	0.004	0.093 ± 0.017	0.092	1.3 ± 0.3	0.177	0.5 ± 0.1
COSMOS2015 $z_{max} = 6$ $w = 0.7$	1	3	0.15 ± 0.10	774^{+203}_{-183}	0.007	0.367 ± 0.129	0.188	2.0 ± 0.7	0.199	1.8 ± 0.7
	2	3	0.35 ± 0.10	694^{+183}_{-163}	0.005	0.015 ± 0.134	0.132	0.1 ± 1.0	0.179	0.1 ± 0.7
	3	3	0.55 ± 0.10	618^{+163}_{-145}	0.005	0.083 ± 0.066	0.104	0.8 ± 0.6	0.168	0.5 ± 0.4
	4	5	0.85 ± 0.20	1035^{+145}_{-114}	0.003	0.067 ± 0.060	0.097	0.7 ± 0.6	0.188	0.4 ± 0.3
	5	8	1.40 ± 0.35	1335^{+114}_{-79}	0.003	0.097 ± 0.032	0.076	1.3 ± 0.4	0.189	0.5 ± 0.2
	6	14	2.40 ± 0.65	1561^{+79}_{-45}	0.003	0.196 ± 0.039	0.055	3.5 ± 0.7	0.180	1.1 ± 0.2
	7	6	3.30 ± 0.25	420^{+45}_{-38}	0.007	0.044 ± 0.024	0.039	1.1 ± 0.6	0.151	0.3 ± 0.2
means:			1.29 ± 0.25	920^{+211}_{-195}	0.005	0.124 ± 0.046	0.099	1.4 ± 0.4	0.179	0.7 ± 0.2

Table 3. Cont.

Sample	j	n	\bar{z}	$\Delta r(z)$, Mpc	σ_p	σ_{obs}	σ_{dm}	b_{dm}	σ_{pl}	b_{pl}
COSMOS2015 $z_{max} = 6$ $w = 0.9$	1	3	0.15 ± 0.10	774^{+203}_{-183}	0.010	0.360 ± 0.203	0.188	1.9 ± 1.1	0.199	1.8 ± 1.0
	2	3	0.35 ± 0.10	694^{+183}_{-163}	0.007	0.066 ± 0.109	0.132	0.5 ± 0.8	0.179	0.4 ± 0.6
	3	3	0.55 ± 0.10	618^{+145}_{-145}	0.006	0.029 ± 0.071	0.104	0.3 ± 0.7	0.168	0.2 ± 0.4
	4	3	1.05 ± 0.10	459^{+121}_{-108}	0.005	0.001 ± 0.109	0.070	0.0 ± 0.0	0.151	0.0 ± 0.0
	5	4	1.50 ± 0.15	538^{+97}_{-83}	0.006	0.059 ± 0.053	0.062	1.0 ± 0.9	0.160	0.4 ± 0.3
	6	4	1.80 ± 0.15	463^{+83}_{-71}	0.007	0.024 ± 0.043	0.054	0.4 ± 0.8	0.154	0.2 ± 0.3
	7	7	2.25 ± 0.30	756^{+71}_{-55}	0.006	0.205 ± 0.065	0.053	3.9 ± 1.2	0.168	1.2 ± 0.4
	8	12	3.10 ± 0.55	1000^{+55}_{-374}	0.006	0.483 ± 0.076	0.045	10.8 ± 1.7	0.168	2.9 ± 0.5
means:			1.34 ± 0.19	663^{+146}_{-130}	0.006	0.153 ± 0.064	0.089	2.7 ± 1.3	0.168	1.0 ± 0.4
COSMOS2015 $z_{max} = 6$ $w = 0.97$	1	3	0.55 ± 0.10	618^{+163}_{-145}	0.008	0.005 ± 0.066	0.104	0.0 ± 0.0	0.168	0.0 ± 0.0
	2	3	0.75 ± 0.10	548^{+145}_{-129}	0.007	0.057 ± 0.067	0.087	0.7 ± 0.8	0.160	0.4 ± 0.4
	3	4	1.20 ± 0.15	633^{+114}_{-97}	0.008	0.063 ± 0.139	0.072	0.9 ± 1.9	0.166	0.4 ± 0.8
	4	13	2.05 ± 0.60	1678^{+92}_{-53}	0.008	0.338 ± 0.080	0.062	5.5 ± 1.3	0.185	1.8 ± 0.4
	5	25	3.85 ± 1.20	1754^{+53}_{-25}	0.014	1.104 ± 0.175	0.040	27.3 ± 4.3	0.170	6.5 ± 1.0
	6	4	5.20 ± 0.15	147^{+25}_{-23}	0.054	0.074 ± 0.087	0.025	2.1 ± 2.4	0.126	0.4 ± 0.5
means:			2.27 ± 0.38	896^{+290}_{-282}	0.017	0.273 ± 0.173	0.065	7.3 ± 4.4	0.162	1.9 ± 1.0

5. Discussion

As we note above, the galaxy bias is a complicated function that can rise with increasing redshift. A theoretical estimate of the dark matter galaxy bias function $b_{dm}(z)$ for the COSMOS field calculated by Equation (15) can be improved by taking into account the stellar mass of the COSMOS galaxies [9]. Thereby our results are consistent with the SCM predictions. Nevertheless, the presence of fluctuations with a high value of the bias (5, 10, or 20) is a direct indication of the existence of large-scale structures that are interesting for the LSSU study.

As we show on Figure 4 (bottom) and Figure A2 (bottom), the larger value of the sampling parameter w leads to the increasing correlation of fluctuations between the COSMOS2015 and the UltraVISTA+deep-UltraVISTA samples. This means that introducing additional sampling criteria for the quality of photometric redshifts of galaxies provides a more reliable fluctuation pattern, which was one of the goals of this work.

Comparison of the physical properties of the objects in the local Universe and at large redshifts requires new available observational spectral bands and instruments for multimessenger ranges (such as neutrino and gravitational waves). Observational cosmology based on multimessenger data allows one to verify existing cosmological models as well as formulating new ones Shirokov et al. [29]. Our method can be used for the analysis of photometric catalogs towards the transient objects (such as supernovae and gamma-ray bursts) detected by neutrino and gravitational-wave detectors.

The works by Nabokov and Baryshev [8], Lovyagin [23], Shirokov et al. [30], Park et al. [31] emphasize the importance of the analysis of the LSSU for the development of modern cosmology, which has become an increasingly important task in the 21st century. The spatial distribution of galaxies reflects both the initial conditions in the early Universe and the evolution of primordial density perturbations. The analysis of fluctuations in the radial distribution of galaxies allows one to estimate the sizes and amplitudes of the largest structures in a given sample of galaxies.

Super-large fractal-like structures with scales of more than 100 Mpc reveal themselves both in the spatial distribution of galaxies in the local Universe at redshifts of $z \lesssim 0.1$ and in the quasars and gamma-ray bursts distributions at redshifts of $z \sim 2$ [3,25,30,32–35]. The analysis of fractal properties [3,32,36] can be used to describe the properties of the large-scale distribution of matter [25,30].

Note that in recent works there were detected several structures in the COSMOS field, which also point to existence of large filamentary structures at $z \sim 0.73$, called the COSMOS wall [10], structures at redshifts of $0.1 < z < 1.2$ [11], voids at $z \sim 2.3$ [12] and massive proto-supercluster at $z \sim 2.45$ [13]. The very large structure of the dark matter with a size of about 1000 Mpc was detected in the COSMOS field by using the method of weak gravitational lensing [14,15].

Our results demonstrated in this paper are consistent with our previous works and have a higher quality of detecting fluctuation structure in redshift space. The positive correlation of fluctuations between independent spectral and photometric surveys of different groups is shown in the work Shirokov et al. [9].

6. Conclusions

We have performed the robust statistical analysis of the new photometric catalog COSMOS2015 and obtained new results, which confirm our preceding works. We have considered the radial fluctuations of the number of galaxies along the line of sight in the photometric redshift space for the optical part of the COSMOS2015 catalog and some of its subsamples. We have calculated the histograms of the number of galaxies in redshift bins, constructed empirical and theoretical approximations for the homogeneous distribution by using the LSM, and performed the comparative analysis of their quality. We have obtained the tables of structures for each sample and for each approximation. The bin size, $\Delta z = 0.1$, was chosen such as to maximize the spatial resolution (at a relatively low level of Poisson noise) and minimize the grid effect for determining photometric redshifts with errors $\sigma_z < 0.021(1+z)$ at high redshifts $3 < z < 6$ [6].

Essential improvements in photometric redshift techniques, using the best SED fitting in the COSMOS field imaged in a large number of filters [6] or deep learning methods [19], allow to reach a redshift uncertainty $\sigma_z = 0.007(1+z)$ at small redshifts, which corresponds to a distance uncertainty of ~ 40 Mpc (at $z \sim 1$). So, in our paper, we present the firmly observed structures at redshift $z \sim 2$ with sizes $l \sim 700$ Mpc, which are larger than the BAO scale $l_{ba0} \sim 100$ Mpc.

We have developed Python software for the line-of-sight analysis based on works by Nabokov and Baryshev [7,8], Shirokov et al. [9], Lovyagin [23]. Our method takes into account the integral values within each bin for all quantities that increase the mathematical rigor and certainty of the results. In this paper, we calculate the structure means as the target variables of the method and use algorithms for determining errors. These features make the method more robust for comparative analysis of different samples of galaxies.

Our analysis confirm the presence of dark matter structures from the paper by Massey et al. [14] at small redshifts. Thus, the observations of visible matter and the observations of dark matter are consistent. Moreover, we have obtained huge structures at high redshifts. These results are consistent with the Λ CDM model, if the corresponding bias is taken into account.

Based on the results of the work, we can draw the following conclusions:

- The method for analyzing radial fluctuations of the number of galaxies along the line of sight (see the last work Shirokov et al. [9]) now takes into account the integral values within each bin for all quantities. That increases the mathematical rigor and certainty of the results. The target variables became more robust for comparative analysis of different samples of galaxies with the developed algorithms for error estimation. The use of logarithmic redshift bins can better take into account the photometric errors. Moreover, the metric bin size in logarithmic scale slightly depends on the redshift. Instead of analytical bias functions, numerical estimates of galaxy biases can be obtained from N-body simulations of the Universe (in a grid of model parameters) or by using the concept of model fractal catalogs, as in Shirokov et al. [30].
- For the case of the theoretical form of approximation of homogeneity in the Λ CDM frameworks, the average standard deviation of detected structures from homogeneity is $\sigma_{\text{mean}}^{\Lambda\text{CDM}} = 0.09 \pm 0.02$, and the average characteristic size of structures is $R_{\text{mean}}^{\Lambda\text{CDM}} = 790 \pm 150$ Mpc. The maximum size of the detected structure is $R_j = 1,754 \pm 40$ Mpc, and the minimum one is $R_j = 147 \pm 24$ Mpc.
- For the case of the empirical approximation of homogeneity, the average standard deviation of detected structures from homogeneity is $\sigma_{\text{mean}}^{\text{empiric}} = 0.08 \pm 0.01$, and the average characteristic size of structures is $R_{\text{mean}}^{\text{empiric}} = 640 \pm 140$ Mpc. The maximum size of the detected structure is $R_j = 2,000 \pm 80$ Mpc, and the minimum one is $R_j = 145 \pm 36$ Mpc.

- We have introduced the selection parameter w to take into account different uncertainty of redshifts $\sigma(z)$. At different values of the parameter w , we have obtained similar results.
- Our calculations show that the observed cosmic variance of radial fluctuations in the number of galaxies can be also described by the PLCF at all redshifts [7,9,25].

The method can be also applied in future observation data of the Transient High-Energy Sky and Early Universe Surveyor (THESEUS) space mission project [37,38] that together with optical ground-based telescopes, e.g., GTC [39] and BTA [29], is aimed to explore the unique capabilities of gamma-ray bursts (GRBs) for cosmology and multimessenger astrophysics. The observed distribution of galaxies along the line of sight gives information about the inhomogeneous distribution of visible matter in the fixed direction in the sky. Statistical analysis of a grid of such fields (towards GRB host-galaxy) will allow one to perform a cosmic tomography of the large-scale distribution of galaxies on the largest optically available scales. The cosmic tomography allows one to constrain precisely cosmology as well as the galaxy structures [8,9,18,29,40].

The codes developed in Python underlying this article are available in the LSA software repository on www.github.com, at DOI: 10.5281/zenodo.4167356.

Author Contributions: Investigation, M.C., S.S.; methodology, M.N., S.S., V.G.; software, M.N., M.C., A.B.; writing—original draft, M.N., S.S.; writing—review and editing, M.C., S.S., V.G. All authors have read and agreed to the published version of the manuscript.

Funding: This research received no external funding.

Acknowledgments: The authors gratefully acknowledge The COSMOS team⁷ for the free online access to the data. We thank the anonymous reviewer for important suggestions that helped us to improve the presentation of our results. We are grateful to Lovyagin N. Yu., Gainutdinov R. I., Parul H. D., and Baryshev Yu. V. for helpful advices and remarks. The work was performed as part of the government contract of the SAO RAS approved by the Ministry of Science and Higher Education of the Russian Federation.

Conflicts of Interest: The authors declare no conflicts of interest.

Abbreviations

The following abbreviations are used in this manuscript:

LSM	least-squares method
LSSU	large-scale structure of Universe
SCM	standard cosmological model (Λ CDM)
PLCF	power-law correlation function

Appendix A

The COSMOS2015 catalogue [6] also contains the UltraVISTA DR2 [41] catalogue data. The columns FLAG_HJMCC and FLAG_DEEP that have been combined into a single UltraVISTA sample. Further, a mutual sampling by the COSMOS and UltraVISTA galaxies have also been done. Further, we analyzed two independent samples: the COSMOS subsample (the optical range) with 184,197 galaxies and the UltraVISTA subsample (the near-IR range) with 40,237 galaxies.

The independence of the samples as well as the coverage of different spectral ranges allows one to conduct their comparative analysis. However, the number of UltraVISTA objects is 5 times less than in the COSMOS so this factor should be taken into account. These samples lie in the same direction on the celestial sphere and hence should give a correlation of density fluctuations.

The method was applied with the parameters $\Delta z = 0.1$, $z_{\max} = (3, 6)$ and without w -sampling by $\sigma(z)$. The corresponding histograms of the radial distribution of galaxies with approximations by the Formulas (3)–(6) and fluctuation patterns are shown in Figures A1 and A2. The dotted lines

⁷ <http://cosmos.astro.caltech.edu/page/the-team>

in the fluctuation patterns (right) show the Poisson noise of level $5\sigma_p$. As can be seen in the figures, the COSMOS sample shows four distinct (exceeding the level of $5\sigma_p$) structures with redshifts: $z = 0.15 \pm 0.10$ (void), $z = 0.40 \pm 0.15$ (cluster), $z = 1.45 \pm 0.30$ (void), and $z = 2.00 \pm 0.25$ (cluster). The UltraVISTA sample gives a somewhat different picture, although there is a positive correlation with the COSMOS sample at $z \lesssim 1$, and shows distinct structures at $z = 2.25 \pm 0.50$ (void) and at $z = 3.65 \pm 0.7$ (cluster).

This result can be explained by the fact that in infrared observations the dust attenuation effects are smaller than in the optical range. Thus, according to the COSMOS2015 catalog data, it can be concluded that optical observations provide rich statistics, and therefore, are useful for the LSSU analysis at redshifts $z \lesssim 1$, while infrared observations have a better quality of statistics (in the sense of redshifts) up to $z \lesssim 6$.

The structure tables corresponding to Figures A1 and A2 are shown in Table A1 for $z_{max} = 3$, and Table A2 for $z_{max} = 6$. The parameter j is the index number of structure, detected by the algorithm. The parameter n shows the number of bins of a given structure (each structure is a sequence of bins with only positive or only negative fluctuations). The parameter \bar{z} shows the average redshift value for the bins of each structure, and the errors can be used to restore the centers of the border bins. The parameter $\Delta r(z)$ gives an estimate of the metric size of the structure (sequence of bins), where the upper and lower limits correspond to the metric size of the border bins. The parameter σ_p is an estimate of the Poisson noise, which is equal to the ratio of unity to the number of all galaxies in the structure. The parameter σ_{obs} shows level of the observed cosmic variance, where the error is the standard deviation from σ_{obs} within the structure. We also include columns for comparing observations with the predictions of theoretical models. The parameter σ_{dm} shows the theoretical variance of the dark matter density in the Λ CDM model frameworks. The next column contains the corresponding galaxy bias b_{dm} , with the errors that are proportional to the errors of the σ_{obs} .

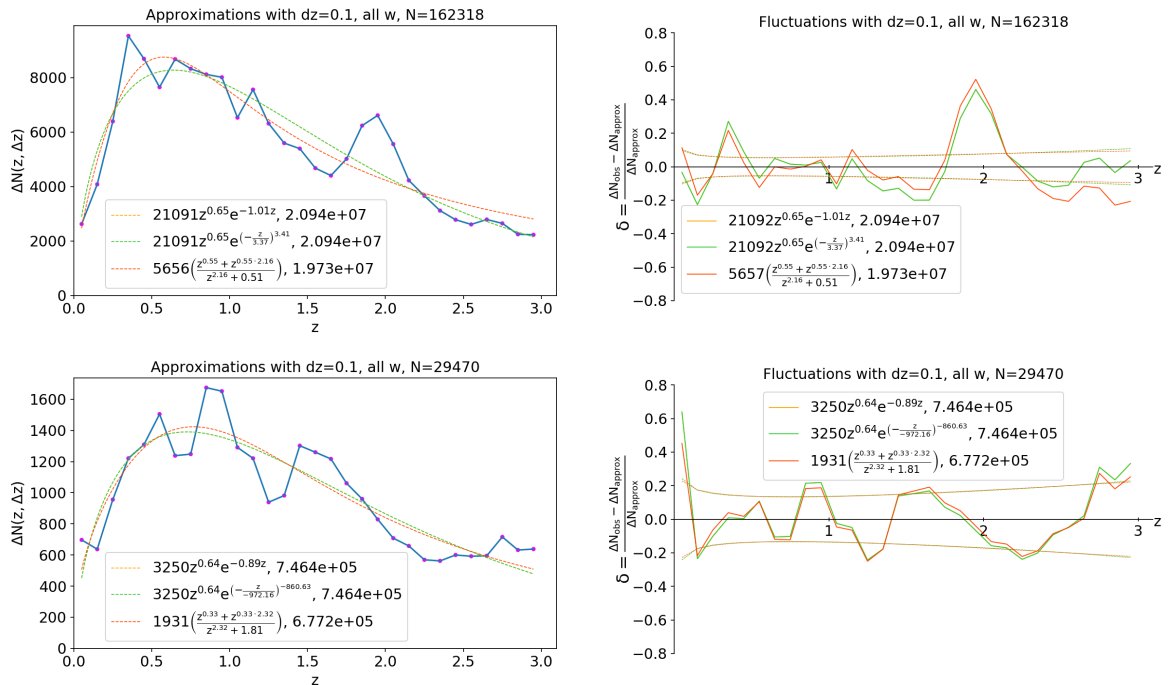


Figure A1. Histograms of the radial distribution of the COSMOS2015 photometric redshifts and corresponding fluctuation patterns for the disjoint 162,318 COSMOS galaxies (**top**) and 29,470 UltraVISTA galaxies (**bottom**) with a bin $\Delta z = 0.1$ and $z_{max} = 3$ without sampling by $\sigma(z)$. The dashed lines indicate the least squares fit (**left**) and Poisson noise 5σ (**right**).

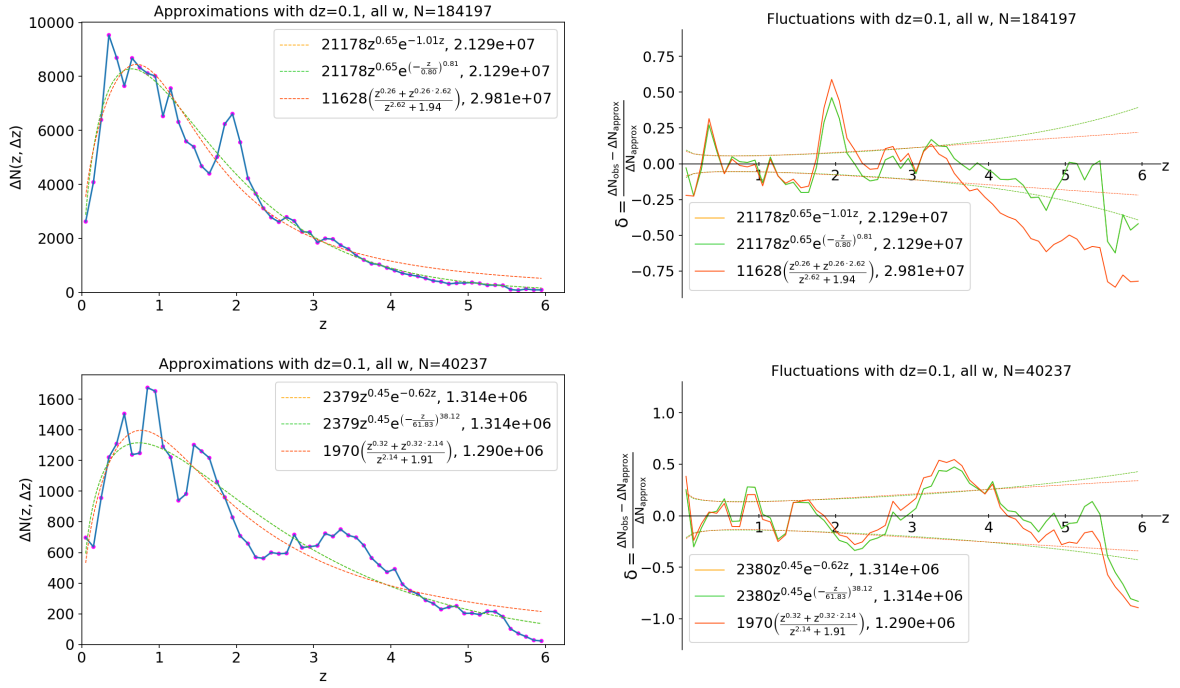


Figure A2. Histograms of radial distribution of the COSMOS2015 photometric redshifts and the corresponding fluctuation patterns for the disjoint COSMOS galaxies (**top**) and UltraVISTA galaxies (**bottom**) with a bin $\Delta z = 0.1$ and $z_{\max} = 6$ without sampling by $\sigma(z)$. The dashed lines indicate the least squares fits (**left**) and Poisson noise 5σ (**right**).

Table A1. Tables of structures for disjoint the COSMOS (top) and UltraVISTA (bottom) samples from the COSMOS2015 catalogue for a bin $\Delta z = 0.1$ with $z_{\max} = 3$ and without σ_z selection. The approximation is by empirical Formula (6). In the last string there are the means of corresponding values (by all structures): mean of redshifts \bar{z}_{mean} , mean of structure sizes in Mpc R_{mean} , mean of Poisson noise level $1\bar{\sigma}_p$, mean of observed cosmic variance σ_{mean} , mean of dark matter variance $\bar{\sigma}_{\text{dm}}$, mean of dark matter bias \bar{b}_{dm} , mean of Peebles correlation function variance $\bar{\sigma}_{\text{pl}}$ and its bias \bar{b}_{pl} (see details in the text).

Sample	j	n	\bar{z}	$\Delta r(z)$, Mpc	σ_p	σ_{obs}	σ_{dm}	b_{dm}	σ_{pl}	b_{pl}
Only COSMOS $z_{\max} = 3$ $w = \text{all}$	1	3	0.15 ± 0.10	774^{+203}_{-183}	0.008	0.100 ± 0.063	0.188	0.5 ± 0.3	0.199	0.5 ± 0.3
	2	4	0.40 ± 0.15	1012^{+183}_{-154}	0.006	0.063 ± 0.078	0.140	0.5 ± 0.6	0.198	0.3 ± 0.4
	3	4	0.80 ± 0.15	799^{+145}_{-121}	0.006	0.025 ± 0.009	0.094	0.3 ± 0.1	0.178	0.1 ± 0.1
	4	3	1.05 ± 0.10	459^{+121}_{-108}	0.007	0.020 ± 0.057	0.070	0.3 ± 0.8	0.151	0.1 ± 0.4
	5	7	1.45 ± 0.30	1111^{+108}_{-79}	0.005	0.105 ± 0.034	0.073	1.4 ± 0.5	0.184	0.6 ± 0.2
	6	6	2.00 ± 0.25	704^{+79}_{-62}	0.006	0.185 ± 0.081	0.056	3.3 ± 1.4	0.168	1.1 ± 0.5
	7	5	2.45 ± 0.20	462^{+62}_{-53}	0.008	0.058 ± 0.030	0.046	1.3 ± 0.6	0.154	0.4 ± 0.2
	8	3	2.75 ± 0.10	204^{+53}_{-49}	0.011	0.014 ± 0.026	0.035	0.3 ± 0.4	0.125	0.1 ± 0.1
means:			1.38 ± 0.17	691^{+166}_{-152}	0.007	0.071 ± 0.021	0.088	1.0 ± 0.4	0.170	0.4 ± 0.1
Only UltraVISTA $z_{\max} = 3$ $w = \text{all}$	1	2	0.10 ± 0.05	397^{+203}_{-193}	0.028	0.202 ± 0.438	0.157	1.3 ± 2.8	0.155	1.3 ± 2.8
	2	3	0.25 ± 0.10	734^{+193}_{-173}	0.018	0.109 ± 0.071	0.155	0.7 ± 0.5	0.187	0.6 ± 0.4
	3	4	0.50 ± 0.15	955^{+145}_{-121}	0.014	0.004 ± 0.044	0.124	0.0 ± 0.0	0.192	0.0 ± 0.0
	4	4	0.90 ± 0.15	753^{+137}_{-114}	0.014	0.077 ± 0.082	0.087	0.9 ± 0.9	0.174	0.4 ± 0.5
	5	5	1.25 ± 0.20	823^{+114}_{-92}	0.013	0.071 ± 0.066	0.075	0.9 ± 0.9	0.176	0.4 ± 0.4
	6	5	1.65 ± 0.20	666^{+92}_{-75}	0.014	0.111 ± 0.028	0.062	1.8 ± 0.4	0.167	0.7 ± 0.2
	7	9	2.25 ± 0.40	1012^{+75}_{-53}	0.012	0.104 ± 0.031	0.055	1.9 ± 0.6	0.175	0.6 ± 0.2
	means:			0.99 ± 0.18	763^{+170}_{-151}	0.016	0.097 ± 0.023	0.102	1.2 ± 0.3	0.175

Table A2. Tables of structures for disjoint the COSMOS (top) and UltraVISTA (bottom) samples from the COSMOS2015 catalogue for a bin $\Delta z = 0.1$ with $z_{\max} = 6$ and without σ_z selection. The approximation is by empirical Formula (6). In the last string there are the means of corresponding values (by all structures): mean of redshifts \bar{z}_{mean} , mean of structure sizes in Mpc R_{mean} , mean of Poisson noise level $1\bar{\sigma}_p$, mean of observed cosmic variance σ_{mean} , mean of dark matter variance $\bar{\sigma}_{\text{dm}}$, mean of dark matter bias \bar{b}_{dm} , mean of Peebles correlation function variance $\bar{\sigma}_{\text{pl}}$ and its bias \bar{b}_{pl} (see details in the text).

Sample	j	n	\bar{z}	$\Delta r(z), \text{Mpc}$	σ_p	σ_{obs}	σ_{dm}	b_{dm}	σ_{pl}	b_{pl}
Only COSMOS	1	3	0.15 ± 0.10	774^{+203}_{-183}	0.008	0.098 ± 0.064	0.188	0.5 ± 0.3	0.199	0.5 ± 0.3
	$z_{\max} = 6$	2	0.40 ± 0.15	1012^{+183}_{-154}	0.006	0.063 ± 0.078	0.140	0.5 ± 0.6	0.198	0.3 ± 0.4
	w = all	3	0.80 ± 0.15	799^{+145}_{-121}	0.006	0.024 ± 0.009	0.094	0.3 ± 0.1	0.178	0.1 ± 0.1
		4	1.05 ± 0.10	459^{+121}_{-108}	0.007	0.021 ± 0.057	0.070	0.3 ± 0.8	0.151	0.1 ± 0.4
		5	1.45 ± 0.30	1111^{+108}_{-79}	0.005	0.106 ± 0.034	0.073	1.5 ± 0.5	0.184	0.6 ± 0.2
		6	2.00 ± 0.25	704^{+79}_{-62}	0.006	0.185 ± 0.081	0.056	3.3 ± 1.4	0.168	1.1 ± 0.5
		7	2.45 ± 0.20	462^{+62}_{-53}	0.008	0.058 ± 0.030	0.046	1.2 ± 0.6	0.154	0.4 ± 0.2
		8	2.75 ± 0.10	204^{+53}_{-49}	0.012	0.016 ± 0.025	0.035	0.3 ± 0.5	0.125	0.1 ± 0.1
		9	3.35 ± 0.30	497^{+45}_{-37}	0.010	0.066 ± 0.032	0.039	1.7 ± 0.8	0.155	0.4 ± 0.2
		10	3.75 ± 0.10	145^{+37}_{-35}	0.017	0.014 ± 0.015	0.028	0.0 ± 0.0	0.118	0.0 ± 0.0
		11	4.45 ± 0.60	717^{+35}_{-25}	0.011	0.128 ± 0.028	0.034	3.7 ± 0.8	0.159	0.8 ± 0.2
		12	5.25 ± 0.10	96^{+24}_{-23}	0.033	0.041 ± 0.036	0.022	1.2 ± 1.0	0.112	0.2 ± 0.2
means:			2.32 ± 0.20	582^{+134}_{-124}	0.011	0.068 ± 0.015	0.069	1.3 ± 0.4	0.158	0.4 ± 0.1
Only UltraVISTA	1	3	0.25 ± 0.10	734^{+193}_{-173}	0.018	0.132 ± 0.095	0.155	0.9 ± 0.6	0.187	0.7 ± 0.5
	$z_{\max} = 6$	2	0.50 ± 0.15	955^{+173}_{-145}	0.014	0.045 ± 0.045	0.124	0.3 ± 0.4	0.192	0.2 ± 0.2
	w = all	3	0.90 ± 0.15	753^{+137}_{-114}	0.014	0.130 ± 0.087	0.087	1.5 ± 1.0	0.174	0.7 ± 0.5
		4	1.25 ± 0.20	823^{+114}_{-92}	0.013	0.056 ± 0.065	0.075	0.7 ± 0.8	0.176	0.3 ± 0.4
		5	1.60 ± 0.15	511^{+92}_{-79}	0.015	0.101 ± 0.028	0.059	1.7 ± 0.5	0.158	0.6 ± 0.2
		6	2.25 ± 0.50	1271^{+79}_{-51}	0.010	0.175 ± 0.039	0.057	3.1 ± 0.7	0.179	1.0 ± 0.2
		7	2.85 ± 0.10	197^{+51}_{-47}	0.022	0.002 ± 0.023	0.035	0.0 ± 0.0	0.124	0.0 ± 0.0
		8	3.65 ± 0.70	1063^{+47}_{-30}	0.012	0.249 ± 0.041	0.040	6.2 ± 1.0	0.166	1.5 ± 0.3
		9	4.60 ± 0.25	285^{+30}_{-26}	0.024	0.043 ± 0.029	0.030	1.2 ± 0.8	0.143	0.3 ± 0.2
		10	5.00 ± 0.15	154^{+26}_{-24}	0.033	0.061 ± 0.032	0.025	2.0 ± 1.0	0.127	0.4 ± 0.2
		11	5.30 ± 0.15	143^{+24}_{-23}	0.036	0.044 ± 0.045	0.024	1.0 ± 1.1	0.126	0.2 ± 0.2
means:			2.56 ± 0.24	626^{+150}_{-141}	0.019	0.094 ± 0.023	0.065	1.9 ± 0.5	0.159	0.6 ± 0.1

The next column contains the approximation of the matter density σ_{pl} , distributed according to the PLCF with the parameters ($r_0 = 5, \gamma = 1.0$) (see Tables 3 and 4 in Shirokov et al. [9]). At high redshifts ($z > 3.6$), linear extrapolation of the data in logarithmic coordinates was used to determine σ_{pl} . Column b_{pl} contains the corresponding bias parameter, where errors are calculated in the same ways as b_{dm} . The bias value $b = 0$ indicates that the Poisson noise is higher than σ_{obs} , and this structure is excluded from the $b(z)$ function, as well as from the calculation of the average bias value b_{mean} .

Last row contains the following average values of corresponding parameters over all structures detected in a sample of galaxies: average redshift \bar{z}_{mean} , average size of structures in Mpc R_{mean} , average Poisson noise level $1\bar{\sigma}_p$, average observed cosmic variance σ_{mean} , average dark matter variance $\bar{\sigma}_{\text{dm}}$, average dark matter bias \bar{b}_{dm} , average Peebles correlation function variance $\bar{\sigma}_{\text{pl}}$ and its bias \bar{b}_{pl} . Errors of all the target values correspond to the standard deviation of the corresponding parameters for all structures, except for σ_{mean} , which is calculated by the Formula (12).

The catalogue contains an interesting note about redshift columns: “a comparison photo-z/spec-z shows that these errors could be underestimated by a factor $0.1 * I - 0.8$ at $I > 20$ and 1.2 at $I < 20$ ”. Taking this into account one can improve the picture of spatial structures of the catalog and enhance the correlation of density fluctuations between independent surveys of this field in future studies.

Appendix B

Figure A3 shows an example of the histogram of radial distribution of galaxies in the metric space (in comoving coordinate system) calculated in the SCM frameworks with parameters ($H_0 = 70, \Omega_v = 0.7$). The transition from catalogs of redshifts to catalogs of metric distances on a grid of models will be possible

with more complete statistics of galaxies obtained by narrow-angle deep surveys like the COSMOS. In the future, this approach could impose new restrictions on cosmological parameters obtained by the cosmic tomography (e.g., Nabokov and Baryshev [8], Shirokov et al. [29], Baryshev et al. [40]).

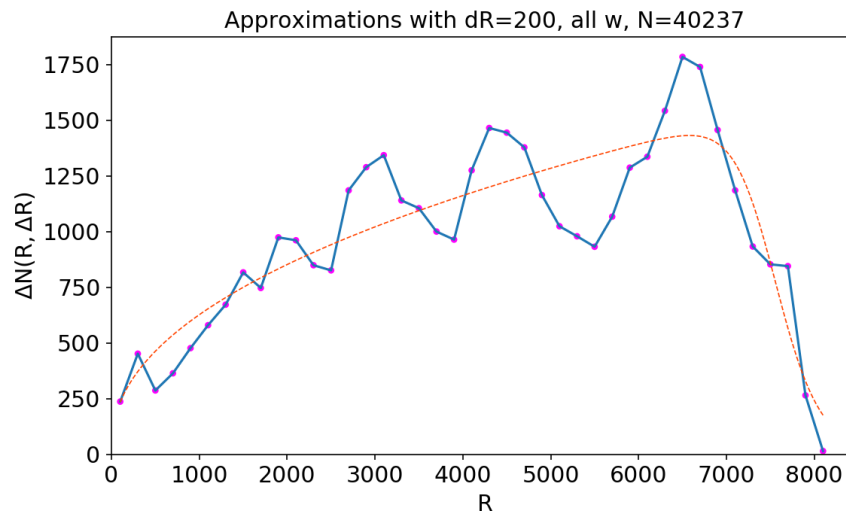


Figure A3. Histogram of radial distribution of the Deep-UltraVISTA [6] photometric redshifts recalculated to metric distances in comoving space with a bin $\Delta R = 200$ Mpc without sampling by $\sigma(z)$. The dashed line indicates the least-squares fit by the theoretical approximation of homogeneity (according to the SCM) by Equation (3).

References

1. Peebles, P.J.E. *Principles of Physical Cosmology*; Princeton University Press: Princeton, NJ, USA, 1993.
2. Lukash, V.; Mikheeva, E. *Physical Cosmology*; Physmathlit: Moscow, Russia, 2010; p. 404.
3. Baryshev, Y.; Teerikorpi, P. *Fundamental Questions of Practical Cosmology: Exploring the Realm of Galaxies*; Springer: Berlin, Germany, 2012. [CrossRef]
4. Moster, B.P.; Somerville, R.S.; Newman, J.A.; Rix, H.W. A Cosmic Variance Cookbook. *Astrophys. J.* **2011**, *731*, 113. [CrossRef]
5. Knebe, A.; Stoppacher, D.; Prada, F.; Behrens, C.; Benson, A.; Cora, S.A.; Croton, D.J.; Padilla, N.D.; Ruiz, A.N.; Sinha, M.; et al. MultiDark-Galaxies: Data release and first results. *Mon. Not. R. Astron. Soc.* **2018**, *474*, 5206–5231. [CrossRef]
6. Laigle, C.; McCracken, H.J.; Ilbert, O.; Hsieh, B.C.; Davidzon, I.; Capak, P.; Hasinger, G.; Silverman, J.D.; Pichon, C.; Coupon, J.; et al. The COSMOS2015 catalog: Exploring the $1 < z < 6$ universe with half a million galaxies. *Astrophys. J. Suppl. Ser.* **2016**, *224*, 24. [CrossRef]
7. Nabokov, N.V.; Baryshev, Y.V. Method for analyzing the spatial distribution of galaxies on gigaparsec scales. I. initial principles. *Astrophysics* **2010**, *53*, 91. [CrossRef]
8. Nabokov, N.V.; Baryshev, Y.V. Method for analyzing the spatial distribution of galaxies on gigaparsec scales. II. Application to a grid of the HUDF-FDF-COSMOS-HDF surveys. *Astrophysics* **2010**, *53*, 101. [CrossRef]
9. Shirokov, S.I.; Lovyagin, N.Y.; Baryshev, Y.V.; Gorokhov, V.L. Large-Scale Fluctuations in the Number Density of Galaxies in Independent Surveys of Deep Fields. *Astron. Rep.* **2016**, *60*, 563. [CrossRef]
10. Iovino, A.; Petropoulou, V.; Scodreggio, M.; Bolzonella, M.; Zamorani, G.; Bardelli, S.; Cucciati, O.; Pozzetti, L.; Tasca, L.; Vergani, D.; et al. An high definition view of the COSMOS Wall at $z \sim 0.73$. *Astron. Astrophys.* **2016**, *592*, A78. [CrossRef]
11. Darvish, B.; Mobasher, B.; Martin, D.C.; Sobral, D.; Scoville, N.; Stroe, A.; Hemmati, S.; Kartaltepe, J. Cosmic Web of Galaxies in the COSMOS Field: Public catalogue and Different Quenching for Centrals and Satellites. *Astrophys. J.* **2017**, *837*, 16. [CrossRef]
12. Krolewski, A.; Lee, K.G.; White, M.; Hennawi, J.F.; Schlegel, D.J.; Nugent, P.E.; Lukić, Z.; Stark, C.W.; Koekemoer, A.M.; Le Fèvre, O.; et al. A Detection of $z \sim 2.3$ Cosmic Voids from 3D Lyman- α Forest Tomography In The Cosmos Field. *Astrophys. J.* **2018**, *861*, 60. [CrossRef]

13. Cucciati, O.; Lemaux, B.; Zamorani, G.; Le Fèvre, O.; Tasca, L.; Hathi, N.; Lee, K.G.; Bardelli, S.; Cassata, P.; Garilli, B.; et al. The progeny of a Cosmic Titan: A massive multicomponent proto-supercluster in formation at $z = 2.45$ in VUDS. *Astron. Astrophys.* **2018**, *619*, A49. [[CrossRef](#)]
14. Massey, R.; Rhodes, J.; Ellis, R.; Scoville, N.; Leauthaud, A.; Finoguenov, A.; Capak, P.; Bacon, D.; Aussel, H.; Kneib, J.P.; et al. Dark matter maps reveal cosmic scaffolding. *Nature* **2007**, *445*, 286–290. [[CrossRef](#)] [[PubMed](#)]
15. Massey, R.; Rhodes, J.; Leauthaud, A.; Capak, P.; Ellis, R.; Koekemoer, A.; Réfrégier, A.; Scoville, N.; Taylor, J.E.; Albert, J.; et al. COSMOS: 3D weak lensing and the growth of structure. *Astrophys. J. Suppl. Ser.* **2007**, *172*, 239. [[CrossRef](#)]
16. Scolnic, D.; Perlmutter, S.; Aldering, G.; Brout, D.; Davis, T.; Filippenko, A.; Foley, R.; Hlozek, R.; Hounsell, R.; Jha, S.; et al. The Next Generation of Cosmological Measurements with Type Ia Supernovae. Astro2020: Decadal Survey on Astronomy and Astrophysics. Science White Papers, No. 270. *arXiv* **2019**, arXiv:1903.05128.
17. Shirokov, S.I.; Sokolov, I.V.; Lovyagin, N.Y.; Amati, L.; Baryshev, Y.V.; Sokolov, V.V.; Gorokhov, V.L. High Redshift Long Gamma-Ray Bursts Hubble Diagram as a Test of Basic Cosmological Relations. *Mon. Not. R. Astron. Soc.* **2020**, *496*, 1530. [[CrossRef](#)]
18. Sokolov, I.V.; Castro-Tirado, A.J.; Zhelenkova, O.P.; Solovyev, I.A.; Verkhodanov, O.V.; Sokolov, V.V. The Excess Density of Field Galaxies near $z = 0.56$ around the Gamma-Ray Burst GRB021004 Position. *Astrophys. Bull.* **2018**, *73*, 111–123. [[CrossRef](#)]
19. Pasquet, J.; Bertin, E.; Treyer, M.; Arnouts, S.; Fouchez, D. Photometric redshifts from SDSS images using a convolutional neural network. *Astron. Astrophys.* **2019**, *621*, A26. [[CrossRef](#)]
20. Chiang, Y.K.; Overzier, R.; Gebhardt, K. Discovery of a Large Number of Candidate Protoclusters Traced by 15 Mpc-scale Galaxy Overdensities in COSMOS. *Astrophys. J. Lett.* **2014**, *782*, L3. [[CrossRef](#)]
21. Graziani, L.; de Bennassuti, M.; Schneider, R.; Kawata, D.; Salvadori, S. The history of the dark and luminous side of Milky Way-like progenitors. *Mon. Not. R. Astron. Soc.* **2017**, *469*, 1101–1116. [[CrossRef](#)]
22. Ilbert, O.; Capak, P.; Salvato, M.; Aussel, H.; McCracken, H.; Sanders, D.; Scoville, N.; Kartaltepe, J.; Arnouts, S.; Le Floch, E.; et al. COSMOS photometric redshifts with 30-bands for 2-deg². *Astrophys. J.* **2009**, *690*, 1236. [[CrossRef](#)]
23. Lovyagin, N.Y. Statistical Properties of the Spatial Distribution of Galaxies. *Astrophys. Bull.* **2009**, *64*, 217–228. [[CrossRef](#)]
24. Korn, G.A.; Korn, T.M. *Mathematical Handbook for Scientists and Engineers: Definitions, Theorems, and Formulas for Reference and Review*; McGraw Hill Book Company: New York, NY, USA, 1968.
25. Tekhanovich, D.I.; Baryshev, Y.V. Global Structure of the Local Universe according to 2MRS Survey. *Astrophys. Bull.* **2016**, *71*, 155. [[CrossRef](#)]
26. Sylos Labini, F.; Vasilyev, N.L. Extension and estimation of correlations in cold dark matter models. *Astron. Astrophys.* **2008**, *477*, 381–395. [[CrossRef](#)]
27. Park, C.; Choi, Y.Y.; Kim, J.; Gott, J.R., III; Kim, S.S.; Kim, K.S. The challenge of the largest structures in the universe to cosmology. *Astrophys. J. Lett.* **2012**, *759*, L7. [[CrossRef](#)]
28. Bhowmick, A.K.; Di Matteo, T.; Feng, Y.; Lanusse, F. The clustering of $z > 7$ galaxies: Predictions from the BLUETIDES simulation. *Mon. Not. R. Astron. Soc.* **2018**, *474*, 5393–5405. [[CrossRef](#)]
29. Shirokov, S.I.; Sokolov, I.V.; Vlasyuk, V.V.; Amati, L.; Sokolov, V.V.; Baryshev, Y.V. THESEUS–BTA cosmological tests using Multimessenger Gamma-Ray Bursts observations. *Astrophys. Bull.* **2020**, *75*, 207–218. [[CrossRef](#)]
30. Shirokov, S.I.; Raikov, A.A.; Baryshev, Y.V. Spatial Distribution of Gamma-Ray Burst Sources. *Astrophysics* **2017**, *60*, 484–496. [[CrossRef](#)]
31. Park, C.G.; Hyun, H.; Noh, H.; Hwang, J.C. The cosmological principle is not in the sky. *Mon. Not. R. Astron. Soc.* **2017**, *469*, 1924–1931. [[CrossRef](#)]
32. Gabrielli, A.; Sylos Labini, F.; Joyce, M.; Pietronero, L. *Statistical Physics for Cosmic Structures*; Springer: Berlin, Germany, 2005. [[CrossRef](#)]
33. Courtois, H.M.; Pomarède, D.; Tully, R.B.; Hoffman, Y.; Courtois, D. Cosmography of the Local Universe. *Astron. J.* **2013**, *146*, 69. [[CrossRef](#)]

34. Einasto, M.; Lietzen, H.; Gramann, M.; Tempel, E.; Saar, E.; Liivamägi, L.J.; Juhan, L.; Heinämäki, P.; Nurmi, P.; Einasto, J.; et al. Sloan Great Wall as a complex of superclusters with collapsing cores. *Astron. Astrophys.* **2016**, *595*, A70. [[CrossRef](#)]
35. Lietzen, H.; Tempel, E.; Liivamägi, L.J.; Montero-Dorta, A.; Einasto, M.; Streblyanska, A.; Maraston, C.; Rubiño-Martín, J.A.; Saar, E. Discovery of a massive supercluster system at $z \sim 0.47$. *Astron. Astrophys.* **2016**, *588*, L4. [[CrossRef](#)]
36. Mandelbrot, B.B. *The Fractal Geometry of Nature*; W. H. Freeman and Company: San Francisco, CA, USA, 1982.
37. Amati, L.; O'Brien, P.; Götz, D.; Bozzo, E.; Tenzer, C.; Frontera, F.; Ghirlanda, G.; Labanti, C.; Osborne, J.P.; Stratta, G.; et al. The THESEUS space mission concept: Science case, design and expected performances. *Adv. Space Res.* **2018**, *62*, 191–244. [[CrossRef](#)]
38. Stratta, G.; Ciolfi, R.; Amati, L.; Bozzo, E.; Ghirlanda, G.; Maiorano, E.; Nicastro, L.; Rossi, A.; Vinciguerra, S.; Frontera, F.; et al. THESEUS: A key space mission concept for Multi-Messenger Astrophysics. *Adv. Space Res.* **2018**, *62*, 662–682. [[CrossRef](#)]
39. Castro-Tirado, A.J.; Gorosabel, J.; Castro Cerón, J.M. The study of gamma-ray bursts and their host galaxies in the GTC era. *Revista Mexicana de Astronomía y Astrofísica* **2003**, *16*, 245–248.
40. Baryshev, Y.V.; Sokolov, I.V.; Moskvitin, A.S.; Fatkhullin, T.A.; Nabokov, N.V.; Kumar, B. Study of faint galaxies in the field of GRB021004. *Astrophys. Bull.* **2010**, *65*, 311–325. [[CrossRef](#)]
41. McCracken, H.; Milvang-Jensen, B.; Dunlop, J.; Franx, M.; Fynbo, J.; Le Fèvre, O.; Holt, J.; Caputi, K.; Goranova, Y.; Buitrago, F.; et al. UltraVISTA: A new ultra-deep near-infrared survey in COSMOS. *Astron. Astrophys.* **2012**, *544*, A156. [[CrossRef](#)]

Publisher's Note: MDPI stays neutral with regard to jurisdictional claims in published maps and institutional affiliations.



© 2020 by the authors. Licensee MDPI, Basel, Switzerland. This article is an open access article distributed under the terms and conditions of the Creative Commons Attribution (CC BY) license (<http://creativecommons.org/licenses/by/4.0/>).